Characterization of Link Quality Fluctuation in Mobile Wireless Sensor Networks

JIANJUN WEN and WALTENEGUS DARGIE, Technische Universität Dresden, Germany

Wireless sensor networks accommodating the mobility of nodes will play important roles in the future. In residential, rehabilitation, and clinical settings, sensor nodes can be attached to the body of a patient for long-term and uninterrupted monitoring of vital biomedical signals. Likewise, in industrial settings, workers as well as mobile robots can carry sensor nodes to augment their perception and to seamlessly interact with their environments. Nevertheless, such applications require reliable communications as well as high throughput. Considering the primary design goals of the sensing platforms (low-power, affordable cost, large-scale deployment, longevity, operating in the ISM band), maintaining reliable links is a formidable challenge. This challenge can partially be alleviated if the nature of link quality fluctuation can be known or estimated on time. Indeed, higher-level protocols such as handover and routing protocols rely on knowledge of link quality fluctuation to seamlessly transfer communication to alternative routes when the quality of existing routes deteriorates. In this article, we present the result of extensive experimental study to characterise link quality fluctuation in mobile environments. The study focuses on slow movements ($<5\ \mathrm{km\,h^{-1}}$) signifying the movement of people and robots and transceivers complying to the IEEE 802.15.4 specification. Hence, we deployed mobile robots that interact with strategically placed stationary relay nodes. Our study considered different types of link quality characterisation metrics that provide complementary and useful insights. To demonstrate the usefulness of our experiments and observations, we implemented a link quality estimation technique using a Kalman Filter. To set up the model, we employed two link quality metrics along with the statistics we established during our experiments. The article will compare the performance of four proposed approaches with ours.

CCS Concepts: • **Computer systems organization → Sensor networks**; • **Networks → Network protocol design**; **Network measurement**;

Additional Key Words and Phrases: Handover, link quality fluctuation, mobility, wireless links, wireless sensor networks

ACM Reference format:
Jianjun Wen and Waltenegus Dargie. 2021. Characterization of Link Quality Fluctuation in Mobile Wireless Sensor Networks. *ACM Trans. Cyber-Phys. Syst.* 5, 3, Article 28 (April 2021), 24 pages.
https://doi.org/10.1145/3448737

This work has been partially funded by the Sächsische AufbauBank (SAB) under Grand No.: 100369691.
Authors' addresses: J. Wen and W. Dargie, Technische Universität Dresden, Dresden, Germany; emails: {jianjun.wen, waltenegus.dargie}@tu-dresden.de.

2378-962X/2021/04-ART28 $15.00
https://doi.org/10.1145/3448737

1 INTRODUCTION

Emerging wireless sensing platforms promise to play important roles in our everyday life. Integrating sensing, processing, and wireless communication capabilities, these platforms enable remote, affordable, flexible, and long-term monitoring. For example, they can be implanted in or carried by patients who can freely move and carry out everyday activities whilst vital biomedical data are being gathered from them [36, 41]. In addition, the platforms can establish a wireless sensor network enabling the bidirectional flow of data and commands, thus allowing doctors and health assistants to monitor and assist their patients at any time [5, 14, 20].

The success of these platforms chiefly depends on their capacity to establish reliable communication links when they are mobile [40, 49]. This is because the quality of the radio link affects almost all higher-level protocols and services [29, 48]. Due to the low-cost, low-power features, the radio transceivers are often prone to background noise, interference, multi-path fading, shadowing and additional environmental dynamics such as the movement of surrounding people and objects. Furthermore, imperfections and slight variations in hardware design and production (such as the placement of antennae in sensor nodes) introduce unforeseeable irregularities in the radio propagation in different directions. Additional factors such as the effect of human body and undesirable vibrations further exacerbate link quality fluctuation.

Over the past decade, a large number of experimental studies have been conducted to investigate and characterise the link quality of low-power radios and how they affect the performance of communication protocols [1, 17, 42, 43]. Most of these studies, however, focus on static scenarios where the nodes are, by and large, stationary once they are deployed. By contrast, little has been done to characterise the impact of mobility on link quality fluctuation and what factors have to be taken into account when designing mobility-aware **Medium Access Control (MAC)** and routing protocols. In this article, we present the results of extensive experiments pertaining to link quality fluctuation in mobile environments, both indoors and outdoors, focusing on low-speed movements signifying the movement of people in residential and work environments as well as of robots in industrial settings.

The contributions of this article are summarised as follows:

- Reliable and reproducible data collection strategy in different indoor and outdoor settings (foyer, corridor, pathway, lawn).
- Characterisation of link quality fluctuations using different metrics, namely, **Received Signal Strength Indicator (RSSI)**, **Link Quality Indicator (LQI)**, **Packet Delivery Ratio (PDR)**, Continuous Success, and **Continuous Failure (CF)** pertaining to packet transmission.
- Employment of empirical probability density functions to make the analysis and interpretation of statistics comprehensible.
- Design and implementation of a seamless handover mechanism to demonstrate the significance of link quality characterisation.

The remaining part of this article is organised as follows: In Section 2, we explain our experimental setting. In Section 3, we explain our methodology. In Section 4, we compare link quality fluctuations in static and mobile deployments. In Section 5, we characterise link fluctuation in mobile environments using different link quality metrics and probability density functions. In Section 6, we employ two link quality estimation metrics and the statistics we gathered to estimate link quality fluctuation in a mobile setting. The purpose is to support a seamless handover. This section also compares the performance of our approach with four proposed approaches. Finally, in Section 8, we make concluding remarks.

2 BACKGROUND

Existing empirical studies on the characteristics of low-power wireless links suggest that they are dynamic and affected by temporal and spacial factors, such as temperature and surrounding environments, among others. The differences in experimental environments, devices and parameter settings often result in different observations and conclusions [23, 25, 29, 38, 43]. Some of the metrics these studies use to quantify and characterize link quality fluctuation are the following:

- **RSSI:** It is a measure of the received signal power in dBm. It is estimated over eight symbols period of time (128 μs) in the CC2420 radio chip [21], which is the widely used radio chip in the wireless sensor networks community. The RSSI can be read directly from an 8-bit, signed 2's complement register.
- **Signal to Noise Ratio (SNR):** It is an enhanced metric used to measure the link quality by taking the background noise into consideration. It is defined as the ratio of the received signal strength to the background noise. When there is no incoming signal, the value read from the RSSI register represents the background noise. Hence, SNR can be simply calculated as:

$$SNR[dB] = RSSI - Noise. \tag{1}$$

- **LQI:** It is a link quality metric defined in the IEEE-802.15.4 specification [7, 17, 50] and is a characterization of the strength and quality of the received packet. Radio vendors implement it slightly differently. For example, in CC2420, the LQI is an averaged correlation value that is determined from the first eight symbols of each incoming packet and ranges from 50 to 110 [21].
- **Count of Acknowledgement Packets (ACK):** It is a link layer metric indicating that the transmitted packet has been successfully received by the receiver. This metric can be extracted at the sender side when the corresponding acknowledgement packet is successfully received within a specific time following each data transmission.
- **Packet Reception Ratio:** It is a receiver side metric and can be calculated as the ratio of the number of successfully received packets to the number of packets that can be ideally transmitted within a specific time window for a set **Inter Packet Interval (IPI)**. This metric is equivalent to the **Acknowledgement Reception Ratio (ARR)**, a link layer metric at the sender side if one disregards link asymmetry. ARR is sometimes referred to as PDR or **Packet Success Rate (PSR)**. In this article we prefer the term PDR.

Existing studies broadly classify low-power, wireless link into *connected*, *transitional*, and *disconnected* regions [3, 43]. In a *connected* region, the PDR is usually above 90% and communication is regarded as highly reliable and symmetric. Thus, packet losses occur occasionally. In a *transitional* region, the link is bursty (with PDR varying from 10% to 90%) and asymmetric. In a *disconnected* region, the PDR is below 10% and packet loss high. Most practical links in wireless sensor networks supporting mobile nodes are characterised by the *transitional* region.

Miluzzo et al. [30] studied the impact of human body on mobile low-power wireless sensor networks. They conducted experiments in three different environments: large open area, urban, and office environment. The mobile node as transmitter was carried by a human being moving at walking speed and the receiver was deployed statically. Their results showed that the body factor has a significant impact on link quality of low power radios.

Ahmed et al. [2] conducted a series of experiments to study the link characteristics for aerial wireless sensor networks. In their experiments, the TelosB nodes were attached on two UAVs that are flying at the same height and one node was placed on the ground as base station. The communication patterns were bi-directional, which can be classified as ground-to-aerial, aerial-to-ground,

(a) nodes (b) foyer (c) corridor (d) pathway (e) lawn

Fig. 1. Experiment environments for empirical studies on link quality in mobile wireless sensor networks: (a) an example of static and mobile nodes. Indoor: (b) foyer and (c) corridor. Outdoor: (d) pathway and (e) lawn.

and aerial-to-aerial. After analysing RSSI variations with respect to distance and packet loss rate, they concluded that A-A links perform best.

Xiong et al. [48] presented experimental studies on link characteristics of IEEE802.15.4-compliant radio in vehicular communications. In their experiments, one node was attached to a moving car as the transmitter and the other was deployed at the roadside as the receiver. They analysed the link characteristics in terms of RSSI, packet error rate and packet loss distribution with respect to antenna hight, vehicle velocity (30 to 130 km/h), and distance (0 to 600 m) in both line-of-sight and non line-of-sight scenario. The experiment results reveal that the link quality is asymmetric and affected by antenna hight and Doppler effect. Furthermore, the authors remark that the conventional size of the ACK packet is too short to guarantee successful acknowledgement. As a result, the ACK mechanism may consume about 38% of the channel resources in non-line of sight scenarios to achieve reliable communication.

3 METHODOLOGY

We conducted a variety of experiments in different environments and settings to study the impact of mobility on the link quality of wireless sensor networks. We gathered and evaluated most of the link quality metrics we listed in the previous section.

3.1 Platforms

We employed the TelosB [37] and the Imote2 [32] sensor platforms for our experiments. Despite the difference in their hardware architecture, the platforms are widely used by the community and both integrate a Chipcon CC2420 radio chip, which implements the IEEE 802.15.4 specification. The CC2420 has 16 non-overlapping channels in the 2.4-GHz unlicensed ISM band, each channel occupying a 2-MHz bandwidth and has 5-MHz channel spacing [21]. It shares the same wireless spectrum with other wireless technologies like WiFi and Bluetooth. Despite having the same transceiver, the two platforms have different RF engineering designs: the TelosB platform has an on-board printed inverted F-style antenna, whereas the Imote2 platform integrates a 2.4-GHz surface mounted antenna. Unless explicitly specified, the findings presented in this study are generated from both platforms. To avoid inconsistency arising from hardware discrepancy, each experiment was repeated at least 10 times for each hardware platform.

3.2 Testbed and Environments

We employed the MobiLab testbed [45] to control all the experiments. The testbed integrates and controls 16 wireless sensor nodes and 3 mobile robots. Figure 1(a) shows snapshots of our

experiment settings. MobiLab is a scalable, mobility-enabled wireless sensor network testbed that can be easily deployed in different environments. It is suitable for conducting consistent and reproducible experiments using control scripts. The backbone channel of the testbed consists of a WiFi ad-hoc network and remotely controls the experiment, collecting link quality metrics. We employed robots to make sure that experiments could be repeated in a consistent manner and results could be compared objectively.

The experiments were conducted in both indoor and outdoor environments. The indoor environments consist of our faculty's foyer and corridors (refer to Figure 1(b) and (c)). In the outdoor environments, the nodes were deployed on a pathway next to our faculty and on a lawn in a garden (see Figure 1(d) and (e)). During all the experiments, people (mostly students) were moving about and carrying out everyday activities unhindered (in other words, we incurred no special conditions to conduct the experiments).

3.3 System Configuration and Data Collection

The link quality evaluation protocol we developed inherited the default radio stack of CC2420 in the TinyOS environment [27]. For each packet transmission, background noise (before and after each transmission as well as after each reception), RSSI, LQI, ACK, timestamps, and packet sequence numbers were recorded (for more information on how these metrics were stored and transferred during the experiments, refer to Reference [45]). To avoid packet collision, a Time Division Multiple Access protocol was implemented, so that only a single pair of transmitter and receiver was active at any given time. Unless stated otherwise, the wireless sensor nodes attached to the mobile robots were the transmitters and all other nodes in the network were receivers.

In most of the experiments, the transmission power was set to −25 dBm that achieves a radio communication range of up to 30 m in both indoor and outdoor environments, provided that the communication partners maintained a line of sight communication. The reason that this low transmission power was chosen is twofold:

(1) The speed of the mobile platform was approximately 0.13 m/s, so it would take a significantly longer time of travel to experience link disconnection than if a larger transmission power were used, e.g., 0 dBm. By using −25 dBm, the communication range was limited to 30 m. Thus, all the link characteristics (perfect, transitional, disconnected regions [43]) could be observed in a small area.
(2) The maximum coverage of the backbone channel of the MobiLab testbed in outdoor environment was approximately 50 m. We could not use a more powerful WiFi access point, because it would require an AC power supply and additional access points.

In all our experiments, **Cross Technology Interference (CTI)** was not taken into consideration. Nevertheless, to minimize the impact of CTI, the transmission channel was set to 26, which is orthogonal to most widely used WiFi channels[1] (channel 1, 6, 11) [28, 31, 43]. Figure 2 shows the average background noise with error bars in different environments when the experiments were conducted. The background noise is almost consistent (around −95 to −92 dBm) with a little variation, indicating that the impact of CTI is negligible. Thus, in the subsequent analysis, we use RSSI instead of SNR as one of our link quality metrics.

4 STATIC VS. MOBILE LINKS

Existing empirical studies on the characteristics of low power links in wireless sensor networks mostly focus on stationary scenarios [3, 12, 39, 43]. These observations provide useful insights

[1]WiFi channel 1 is used as the testbed backbone channel and in our office building the WiFi channel 6 and 11 are used.

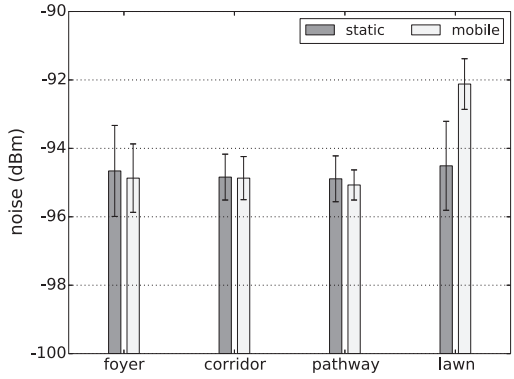

Fig. 2. Background noise in different environments.

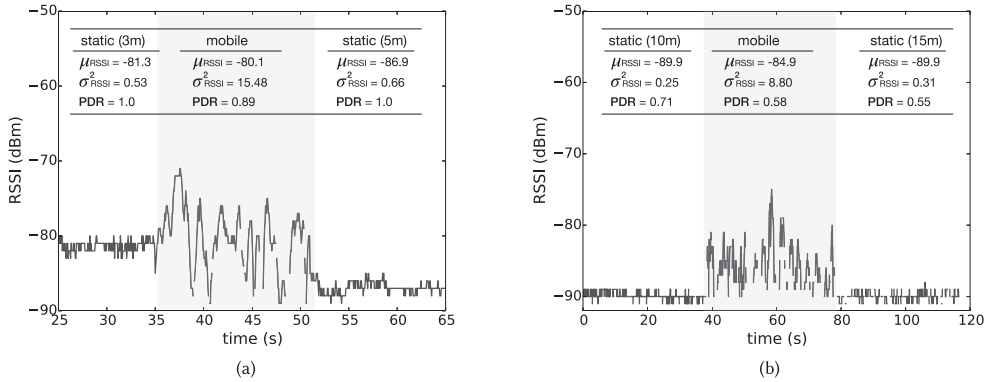

Fig. 3. Comparison of temporal characteristics for static and mobile links. (a) Link fluctuation in the connected region. (b) Link fluctuation in the transitional region.

as to how higher-layer protocols, particularly, MAC and routing protocols, can be optimised for static networks. Nevertheless, their usefulness is limited for designing protocols that support mobile nodes, since the characteristics of mobile links are conspicuously different from their static counterparts, as this study will show.

4.1 Temporal Characteristics

Experiment set-up. In this scenario, a mobile node carried by a robot continuously sends packets to a stationary node with a 50-ms IPI. Initially, the robot was located at a distance of 3 m away from the static receiver and sends packets in burst for about 10 s. After some time, it moved a distance of 2 m in a straight line while sending packets in burst. Then it stopped but continued transmitting packets for another ca. 15 s. The second scenario is similar, however, in this setting, the mobile node began at a different initial location (10 m) and had a longer travelling distance away from the receiver node (5 m). The experiments were conducted in an indoor environment where there was no significant interference.

Observations. Figure 3 compares the temporal characteristics of the static and mobile scenarios. The real-time RSSI fluctuations are presented along with the mean and variance of the RSSI fluctuations that are calculated section by section. Figure 3(a) shows the RSSI fluctuation in a

predominantly connected region where links were stable and the PDR was above 90%. When the transmitter was static (at the locations 3 m and 5 m), the links were stable, so that the PDR was approximately 100% and the RSSI variation was insignificant (having a standard deviation of less than 1 dBm). When the transmitter was mobile (moving from 3 to 5 m), the RSSI fluctuated, such that the standard deviation reached around 4 dBm and the PDR dropped to 89%. Figure 3(b) shows the temporal behaviour of link variations in a predominantly transitional region. As can be seen, it has similar variation patterns as in the previous case. From the above observations, it can be concluded that:

- The RSSI fluctuated appreciably when the transmitter was mobile, regardless of its relative distance to the stationary receiver.
- The fluctuation results in significant packet loss, even when the link is characterised as predominantly connected.

This said, a closer look into the raw RSSI fluctuations in both figures may suggest that on average, the RSSI values of the mobile regions are better than the static regions, which is not the case. We plotted the RSSI values based on received packets. In the mobile cases, we received very few packets whose RSSI values happened to be relatively good. But we have lost many packets whose RSSI values could not be determined. This is one of the reasons why the analysis and interpretation of RSSI values should be made carefully.

4.2 Spatial Characteristics

Experiment set-up. To investigate the spatial characteristics of static and mobile links, we conducted two experiments in an outdoor environment (the lawn). For the static scenario, transmitter nodes were deployed in radial topology, with the receiver node at the centre. For the mobile scenario, the transmitter nodes were carried by robots and moved away from the stationary receiver in eight different directions along radial paths. Figure 5(a) and (b) show our deployment topologies.

Observations. Figure 5(c) and (d) shows the contour plots of RSSI distributions for the static and mobile links, respectively. As can be seen, the RSSI distributions are spatially irregular, regardless of whether the links were static or mobile, suggesting that signal propagation was anisotropic. The radio irregularity phenomenon is confirmed by previous empirical studies on static wireless links [3, 52]. There are three potential causes for this phenomenon:

(a) The omnidirectional antennae did not have the same gain in different directions (due to imperfection in design and manufacturing).
(b) The environment did not have a similar effect in different directions, leading to different path loss patterns.
(c) The signal propagation (transmission power) itself varied over time.

With this in mind, we believe that for the static deployment, the direction-dependent antenna gain was the primary cause of radio irregularity. This is because the experiment was conducted on a lawn where there was no obvious obstacles nearby and the sensor nodes were deployed in a small circular area (5-m radius). To confirm our claim, we deployed two nodes with a spacing of 1 m. One of the nodes was fixed whilst the robot carrying the other node spun at a slow speed (360° in 20 s). Figure 4 shows the plot of the RSSI variation in relation to different antenna directions.

From Figure 5(c) and (d), we observe that the radio irregularity becomes worse when the links were mobile. The RSSI variations are more dynamic compared to the static links, which is also mentioned in the earlier discussion. Although the signal propagation is more irregular, the measured RSSI values are relatively high in all directions in the mobile links. This can be observed in Figure 3, in which the average RSSI in the mobile links is higher than that of in the static links.

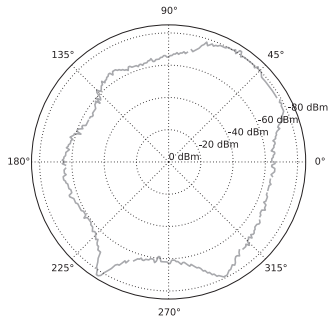

Fig. 4. Radio propagation irregularity. Two nodes are deployed along a line of 1-m spacing. One of them is fixed and the other spins at a speed of 0.05 round per second. Degree 0 is the position that the two antennae face one another.

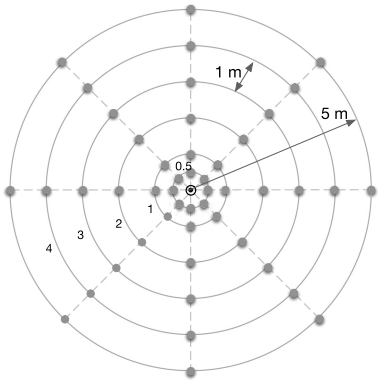

(a) static deployment

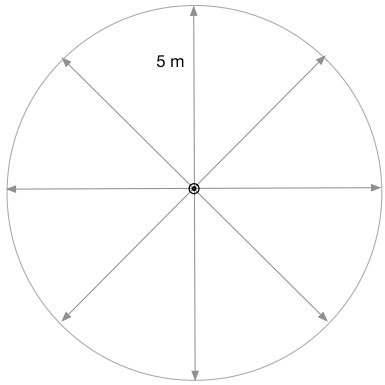

(b) mobile trajectory

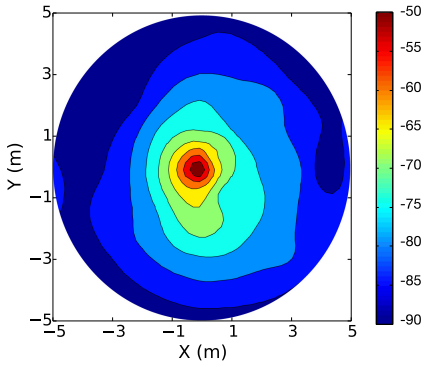

(c) RSSI distribution of static links

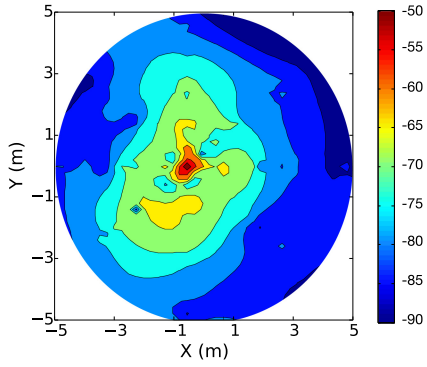

(d) RSSI distribution of mobile links

Fig. 5. Comparison of spatial characteristics of static and mobile links. (a) Static deployment topology: The node at the centre is the receiver and the others are transmitters. (b) Trajectory of the mobile transmitter. The mobile sender moves away from the centre and toward the outer circle along a radial line. (c) Contour of the RSSI distribution for the static links. (d) Contour of the RSSI distribution for the mobile links.

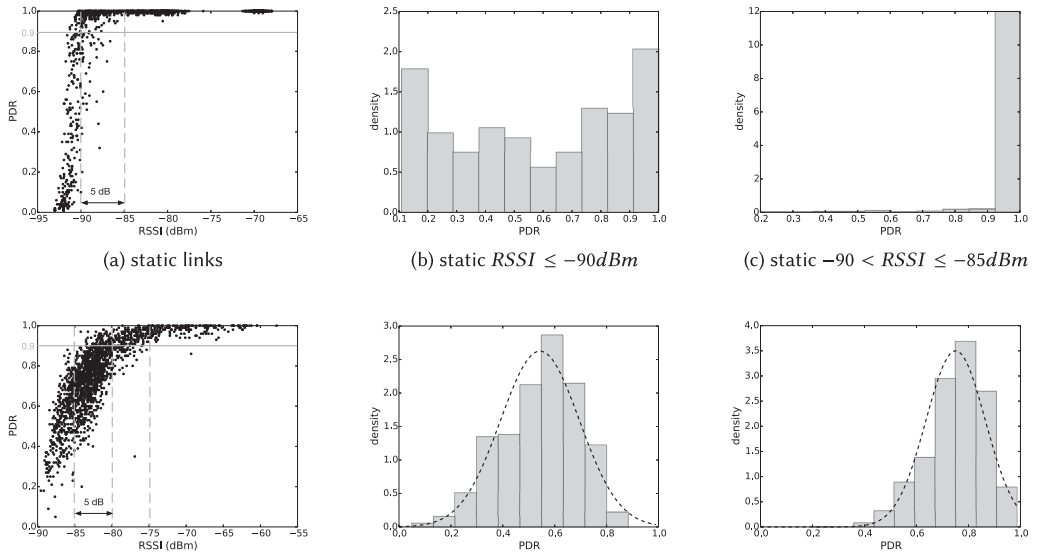

(a) static links (b) static $RSSI \leq -90dBm$ (c) static $-90 < RSSI \leq -85dBm$

(d) mobile links (e) mobile $-90 < RSSI \leq -85dBm$ (f) mobile $-85 < RSSI \leq -80dBm$

Fig. 6. The relationship between RSSI and PDR. The empirical density functions of the PDR are generated for the RSSI of 5-dBm width.

4.3 Relationship between PDR and RSSI

Experiment set-up. The data used for this section are taken from all the experiments we conducted for the comparison of static and mobile links. The PDR is calculated for every 100 successive packets transmitted and the RSSI values shown in the figures are averaged over successful packets.

Observations. Figure 6(a) and (d) show the PDR distributions plotted against the RSSI values for the static and mobile links, respectively. As can be seen, the PDR is above 90% when the average RSSI is greater than −85 dBm in static links. In mobile links, the threshold is −75 dBm. When the average RSSI value is below this threshold, the PDR varies significantly (from 100% to nearly 0%), setting the communication region into a *transitional* region. This empirical threshold is environment dependent. For example, for the same radio chips we used in our experiments, different values have been reported in the past: −75 dBm in Reference [18], −87 dBm in Reference [26], or −80 dBm in Reference [44] to achieve a 90% PDR. In addition to the different RSSI thresholds to separate *connected* from *transitional* regions in static and mobile links, the width of *transitional* region is different. In static links, this width is approximately 10 dBm, while in mobile links it is 5 dBm, much narrower than that of static links.

To further investigate the relationship between PDR and RSSI in the *transitional* region (where the PDR varies from 90% to 10%), we plotted the distribution functions of the PDR for specific RSSI ranges. For the static links, the PDR is almost uniformly distributed when the RSSI is between −95 and −90 dBm whereas for the mobile links, the distribution is more like normal. These features are depicted in Figure 6(b) and (e), respectively. Figure 6(c) and (f) depicts the distributions of PDR for different ranges, each range having a width of 5 dBm. From Figure 6(c), we can observe that when the RSSI was between −90 and −85 dBm in the static links, the PDR was above 90% with a probability of 0.85. In the mobile links, however, the PDR varied between 30% and 100% for relatively larger RSSI values (i.e., −85 dBm < RSSI ≤ −80 dBm). This is shown in Figure 6(f).

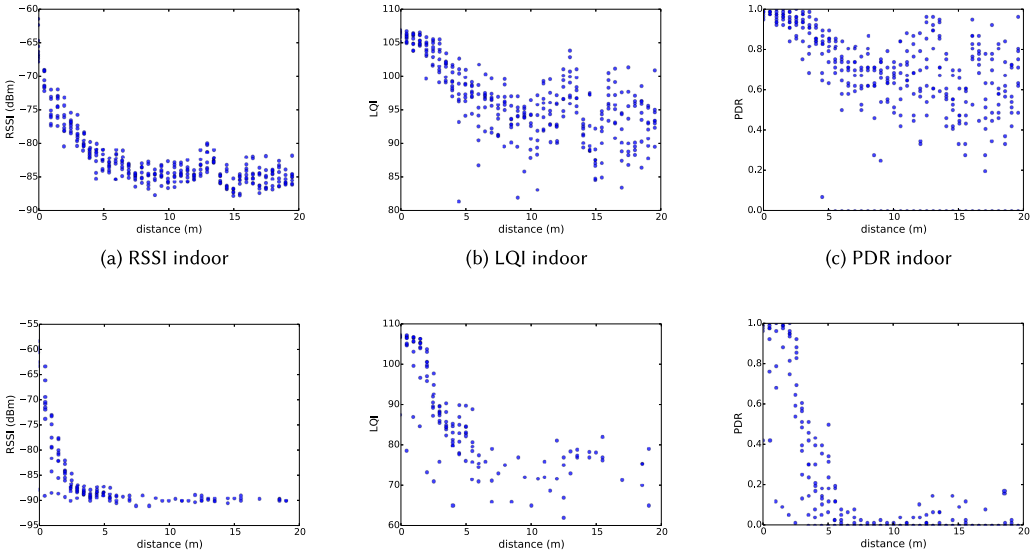

(a) RSSI indoor (b) LQI indoor (c) PDR indoor

(d) RSSI outdoor (e) LQI outdoor (f) PDR outdoor

Fig. 7. Characterisation of link quality fluctuation in indoor and outdoor environments.

5 CHARACTERISTICS OF MOBILE LINKS

In Section 4, we compared the difference in link quality fluctuations between static and mobile links. Although they have similar characteristics, such as non-uniform radio propagation and RSSI variations, the similarities, nevertheless, should not be overstated. In general, links in mobile environments are more dynamic than their static counterparts. In this section, we explore the characteristics of mobile links more closely, taking different perspectives.

5.1 Spatial Characteristics

Experiment set-up. To investigate the spatial characteristics of link quality fluctuation in mobile scenarios, we conducted experiments in indoor (foyer) and outdoor (pathway) environments. For each experiment, one stationary node was deployed as a receiver and a mobile node moved away from the receiver along a straight line to cover a distance of 20 m long. The mobile transmitter sends packets at an IPI of 50 ms. For each scenario, the experiments were repeated 10 times.

Observations. Figure 7 highlights the spatial characteristics in terms of RSSI, LQI, and PDR. All link quality metrics were collected at the sender side. The three figures on top are for the indoor environment and the figures at the bottom are for the outdoor environment. The RSSI and LQI points depicted in the figures are averaged values of 80 successive packets, whereas the PDR was generated by accumulating ACK packets. Figure 7(a) and (d) show RSSI variations along the distance axis. As expected, RSSI decreased while the relative distance between the sender and the receiver increased, following the log-normal path loss model [13] (refer also to Reference [34]):

$$RSSI(d) = RSSI(d_0) - 10 \cdot log_{10}\left(\frac{d}{d_0}\right) + N(0, \sigma^2), \tag{2}$$

where $RSSI(d)$ is the path loss at distance d, $RSSI(d_0)$ is the path loss measured at a reference distance d_0, n represents the path loss exponent and $N(0, \sigma^2)$ is a white-Gaussian noise. The path loss exponent is different for different environments. By applying curve fitting, we can estimate

Table 1. The Correlation Coefficients of PDR and RSSI as Well as PDR and LQI

	$\rho\,(RSSI, PDR)$		$\rho\,(LQI, PDR)$	
slot size	mean	variance	mean	variance
10	0.56	0.002	0.73	0.002
50	0.67	0.003	0.80	0.005
100	0.73	0.005	0.85	0.011

the path loss exponent for our case, which is 0.89 for the indoor environment and 1.12 for the outdoor environment.

From Figure 7(c) and (f), we observe that link quality in terms of PDR is not strictly correlated with distance, although PDR generally decreases with distance increasing. In Figure 7(c), the PDR in the range of 10 to 14 m is higher than that in the range of 5 to 10 m. In the range of 14 to 15 m, the PDR decreases, then after 16 m it increases slightly. In Figure 7(f), we observe the same phenomenon (that farther locations have an improved PDR). Additionally, in the outdoor experiment, the links are almost disconnected after 7 m, whereas in the indoor environment, even after 20 m, the packet success rate was relatively high.[2] Because of the space limitation in our foyer, we could not observe link behaviour beyond 25 m.

By observing the plot shape of the PDR, RSSI, and LQI, we find that PDR is highly correlated with RSSI and LQI. They almost have the same variation tendency. To confirm this argument, we calculated the correlation coefficient of PDR and RSSI, PDR, and LQI by using the following equation:

$$\rho_{x,y} = \frac{cov(x,y)}{\sigma_x \sigma_y}, \tag{3}$$

where $\rho_{x,y}$ is the correlation coefficient of x and y; $cov(x,y)$ represents the covariance between x and y; and ρ_x, ρ_y denote standard deviations, respectively. Table 1 shows the correlation coefficients using different slot sizes to calculate the PDR. When using a larger slot size to calculate the PDR, the correlation coefficient increased. In other words, the PDR is significantly correlated with RSSI and LQI. Another conclusion one can draw from the experiments is that, in mobile links, the *transitional* region is much more broader than the *connected* region. As shown in Figure 7(c), the *connected* region (PDR > 0.9) in the indoor environment is only 3 m long, whereas the *transitional* region is more than 17 m long.[3]

5.2 Packet Consecutive Failure

In Section 5.1, we observed that the correlation for PDR depends on the slot size. In Reference [43], the authors observed that when using a smaller slot size to calculate the PDR, it resulted either in a large number of good or in a large number of poor links. When using a larger slot size, the number of links in the transitional region increases and the number of links in the connected and disconnected regions decreases. To mitigate the bias caused by slot size, we analysed the correlation of CF and RSSI variation. It must be noted that a high CF implies a bad link; and in a bad link, the average RSSI value of the received packets is consistently low (which is reflected by a small variance or a narrow density function).

[2]Our observation appears to contradict the notion that signal propagation is poorer in indoor environments than in outdoor environments due to many factors affecting the signal in indoor environments, such as multi-path effect.
[3]Due to space limitations, the disconnected region could not be observed in the experiment.

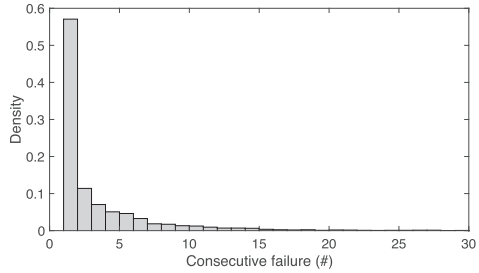

Fig. 8. The density function of consecutive packet failures.

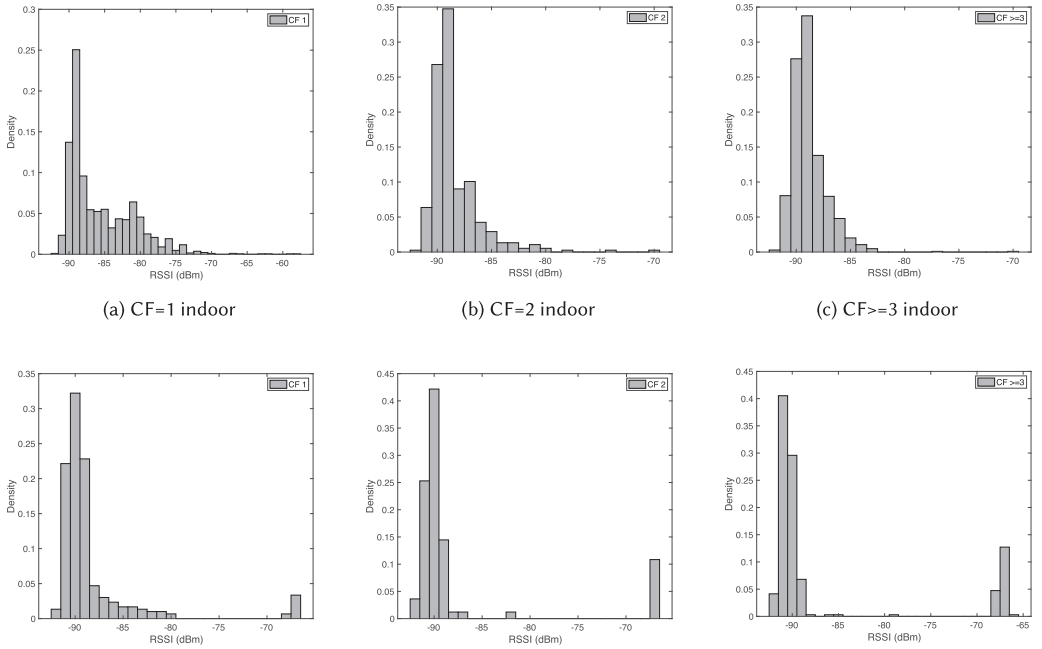

(a) CF=1 indoor (b) CF=2 indoor (c) CF>=3 indoor

(d) CF=1 outdoor (e) CF=2 outdoor (f) CF>=3 outdoor

Fig. 9. The RSSI distribution for specific CF in indoor and outdoor environments.

Experiment set-up. The data analysed in this section are the same as in the previous section. CF is accounted through ACK sequences and RSSI is estimated by averaging the RSSI values of successfully transmitted packets before and after the failure(s).

Observations. Figure 8 shows the density function of consecutive failure in indoor and outdoor environments. We observe that single packet failure occurs more often than multiple consecutive failures. In 95% of the cases, the number of consecutive failures is less than 10. It is most likely that single packet failure is caused by link fluctuations due to mobility. To further analyse the impact of RSSI variations on transmission failures, we plotted the conditional density functions of the RSSI, as shown in Figure 9. Figure 9(a) and (e) show the RSSI distributions when a single packet failure occurs in indoor and outdoor environments, respectively. In the indoor environment, a single packet failure can be observed in a wide range of RSSI, which means that it is difficult to predict CF using RSSI values. In the outdoor environment, the result is almost the same, but within a narrow RSSI range, which is 5 dBm less. From the figures, it should be noted that the probability

of observing a single packet failure increases as RSSI decreases. This observation is applicable for the case where the consecutive failure is larger than 2 (as shown in Figure 9(b) to (f)). From these figures it can be observed that when the link quality is consistently poor (a narrow distribution function), the consecutive failure of packets increases.

6 LINK QUALITY ESTIMATION TO SUPPORT A SEAMLESS HANDOVER

In this section, we shall give account of how we employed some of the experimental results to develop a link quality estimation model for supporting a seamless handover. A seamless handover is useful for applications requiring continuous and highly reliable communication. Typical examples are telemedicine applications such as those monitoring patients with epileptic seizure [6], Parkinson's disease [10], or gastroparesis [19, 22]. The tasks of the handover protocol or algorithm are to (1) continuously evaluate the quality of a wireless link established between a mobile node (typically, worn by a patient) and a nearby stationary relay node and (2) transfer communication in time when the quality deteriorates below an acceptable threshold. The transfer of communication should take place before an existing link breaks completely.

In cellular networks, the task of managing mobility is assigned to resource-rich base stations, which are always powered on and active. In wireless sensor networks, the relay nodes alone cannot assume this responsibility, because, like the mobile nodes, they, too, are resource constrained. Therefore, our goal is to enable a mobile node to continuously assess the quality of an existing link and search for alternative relay nodes in its vicinity. For the complete description of the handover protocol, we refer readers to References [46, 47].

Existing or proposed approaches use different metrics for supporting a seamless handover, the simplest metric being evaluating the RSSI values of received packets (Smart-Hop [16], MobiSense [18], and MX-MAC [51]). This approach implements the least complex mechanism to determine link quality fluctuation but it is also unreliable. In Reference [54], the authors combine two metrics, namely, burst loss (consecutive transmission failure) and packet failure rate. If one of the criteria is fulfilled, then a handover is initiated. In Reference [15], the authors employ Fuzzy Logic to estimate link quality [4]. It takes packet success rate, link asymmetry, link stability, and SNR into consideration and combines additional three metrics (energy, traffic load, and depth level) to support a handover. By carefully studying the characteristics of link quality fluctuation in an industrial environment, Zinonos et al. [53] also propose a handover triggering algorithm that employs a Fuzzy Logic. This approach takes the RSSI values of incoming packets and packet loss rate as its inputs. The output of the algorithm is a trigger decision probability, which, if it falls below a predefined threshold, is used to initiate a handover.

6.1 Kalman Filter as a Link Quality Prediction Model

Whereas combining multiple and complementary metrics is the right approach to estimate link quality fluctuation, we assert, nevertheless, that a much better model than a Fuzzy Logic can be adopted for this task. Link quality fluctuation is inherently stochastic and, therefore, the model dealing with its estimation should also be stochastic. Moreover, the model should be able to update the statistics of its parameters whenever fresh evidence becomes available. In this regard, the **Kalman Filter (KMF)** is a more suitable model. Table 2 lists the main parameters we used to describe the Kalman Filter.

To facilitate the prediction process, we divide time into slots and frames. A frame consists of multiple slots. A link quality prediction is made for a frame, based on the statistics of k freshly received ACK packets and n past frames. In each estimation step, the link quality is expressed as a column vector consisting of an RSSI value and a PDR. To explain our approach, we refer to Figure 10. Suppose the parameters we wish to estimate for the time frame τ can be represented

Table 2. The Main Parameters Used to Describe a Kalman Filter at Time τ

symbol	description
$\mathbf{x}_p[\tau]$	predicted state vector
$\mathbf{x}_m[\tau]$	measured state vector
$\hat{\mathbf{x}}[\tau]$	updated (estimated) state vector
$k[\tau]$	Kalman gain
$\mathbf{w}[\tau]$	process error vector
$\mathbf{v}[\tau]$	measurement error vector
$R[\tau]$	measurement error covariance
$C_p[\tau]$	prediction error covariance
$Q[\tau]$	process error covariance

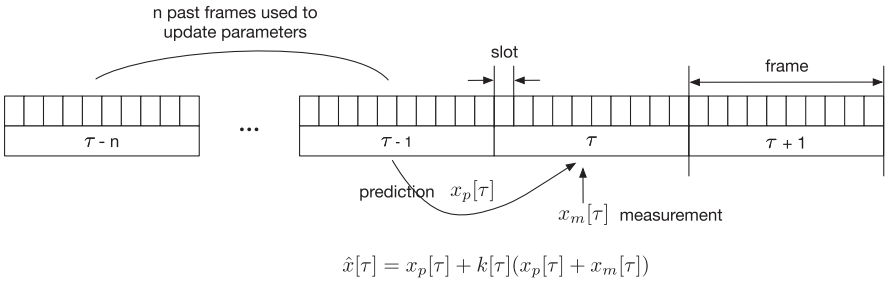

Fig. 10. Connecting the past, present, and future statistics of incoming ACK packets to dynamically update the model parameters of a Kalman Filter.

by the generic random variable $\mathbf{x}[\tau]$. The reason we describe it as a random variable is that we will never be able to obtain its real value at any given time. Suppose, based on the statistics we have gathered up to frame $\tau - 1$ we predict the value of $\mathbf{x}$ for the frame τ and label it as $\mathbf{x}_p[\tau]$. The index p stands for prediction. In the time frame τ, however, we measure the parameters of $\mathbf{x}$ and label this as $\mathbf{x}_m[\tau]$. The index m stands for measurement. Both $\mathbf{x}_p[\tau]$ and $\mathbf{x}_m[\tau]$ contain the actual value of $\mathbf{x}$ for that frame, but each contains a different kind of error, namely, process and measurement error, respectively. Using the Kalman formalism, we can estimate $\mathbf{x}[\tau]$ by properly combining $\mathbf{x}_p[\tau]$ and $\mathbf{x}_m[\tau]$:

$$\hat{\mathbf{x}}[\tau] = \mathbf{x}_p[\tau] + k[\tau]\left(\mathbf{x}_p[\tau] - \mathbf{x}_m[\tau]\right). \tag{4}$$

Note that if the link quality fluctuates slowly over time, then we should trust $\mathbf{x}_p[\tau]$ more. If, however, the link quality fluctuates significantly over time, then we should trust $\mathbf{x}_m[\tau]$ more. How much we should trust either of them at any give τ depends on $k[\tau]$, which should be determined in a dynamic fashion. Moreover, note that:

$$\mathbf{x}_m[\tau] = \mathbf{x}[\tau] + \mathbf{v}[\tau], \tag{5}$$

where $\mathbf{v}[\tau]$ is the measurement error modelled as a random variable. Similarly,

$$\mathbf{x}[\tau] = \mathbf{x}_p[\tau] + \mathbf{w}[\tau], \tag{6}$$

where $\mathbf{w}[\tau]$ is the processor error modelled as a random variable. Hence, our goal should be finding the optimal $k[\tau]$ such that the difference between the actual $\mathbf{x}[\tau]$ and its estimated value, $\hat{\mathbf{x}}[\tau]$, is

minimum. One way to achieve this goal is minimising the mean square error:

$$\mathbf{e}^2[\tau] = E\left\{(\mathbf{x}[\tau] - \hat{\mathbf{x}}[\tau])^2\right\}. \tag{7}$$

If we insert Equation (4) into Equation (7), differentiate the equation with respect to $k[\tau]$, and set the result to 0, then we shall find the optimal $k[\tau]$ that minimises the mean square estimation error [9]:

$$k[\tau] = C_p[\tau]\left(C_p[\tau] + R[\tau]\right)^{-1}, \tag{8}$$

where $R[\tau] = E\left\{\mathbf{v}^2\right\}$ is the measurement error covariance and $C_p[\tau]$ is the prediction error covariance, i.e.,

$$C_p[\tau] = E\left\{\left(\mathbf{x}[\tau] - \mathbf{x}_p[\tau]\right)\left(\mathbf{x}[\tau] - \mathbf{x}_p[\tau]\right)\right\}, \tag{9}$$

which can be expressed as:

$$C_p[\tau] = C[\tau - 1] + Q[\tau], \tag{10}$$

where $C[\tau - 1]$ is the error covariance for $\tau - 1$ and $Q[\tau] = E\{\mathbf{w}^2\}$ is the process error covariance. It is assumed that $\mathbf{v}$ and $\mathbf{w}$ are column vectors consisting of zero mean and normally distributed random variables.

6.2 Defining Model Parameters

Let $\mathbf{x}[\tau]$ be a column vector:

$$\mathbf{x}[\tau] = \left[\mathbf{r}[\tau], \mathbf{p}[\tau]\right]^T, \tag{11}$$

where $\mathbf{r}[\tau]$ is the RSSI value and $\mathbf{p}[\tau]$ the PDR of the τ's frame. Suppose the application wishes to transmits packets continuously, with an IPI of 20 ms. If we fix the size of one packet to 28 B, the transmission rate of the underlying radio chip (CC2420) to 250 kbit s^{-1}, and the maximum speed of the mobile node to 5 km h^{-1} or 1.4 m s^{-1}, the node transmits approximately 47 packets in 1 s (i.e., before it moves a distance of 1.5 m). Furthermore, if we define a slot to be the time we need to receive a single packet and a frame as 10 slots, then we have at least four frames in a second, which we assume are statistically correlated. With this specification, we can express the average RSSI value of the τ's frame in terms of the average RSSI value of the $(\tau - 1)$'s frame:

$$\mathbf{r}[\tau] = \mathbf{r}[\tau - 1] + a. \tag{12}$$

Compared to the fluctuation in RSSI values, the change in the PDR between consecutive frames is small, so that we can assume that:

$$\mathbf{p}[\tau] = \mathbf{p}[\tau - 1]. \tag{13}$$

Putting together these two expressions yields:

$$\begin{bmatrix}\mathbf{r}[\tau] \\ \mathbf{p}[\tau]\end{bmatrix} = \begin{bmatrix}1 & 0 \\ 0 & 1\end{bmatrix}\begin{bmatrix}\mathbf{r}[\tau - 1] \\ \mathbf{p}[\tau - 1]\end{bmatrix} + \begin{bmatrix}a \\ 0\end{bmatrix}, \tag{14}$$

where a is a parameter that can be determined by a linear regression [33] and is associated with the variance in RSSI. The error associated with our assumption as regards $\mathbf{r}[\tau]$ and $\mathbf{p}[\tau]$ can be described as the process error, $Q[\tau]$ and, as such, can be expressed in terms of the variances of $\mathbf{r}$ and $\mathbf{p}$ of the past n frames:

$$\sigma^2_{r,p}[\tau] = \frac{1}{n-1}\sum_{j=(\tau-n-1)}^{\tau-1}(\mathbf{r}[j] - \overline{r})^2, \tag{15}$$

where $\overline{r}$ is average RSSI of the past $n \times k$ slots. Likewise, the process error as regards $\mathbf{p}$ is expressed as:

$$\sigma^2_{p,p}(\tau) = \frac{1}{n-1} \sum_{j=(\tau-n-1)}^{\tau-1} (\mathbf{p}[j] - \overline{p})^2, \tag{16}$$

where $\overline{p}$ is the average PDR of the past n frames. The process error of $\mathbf{x}[\tau]$ expressed as a matrix is

$$Q(\tau) = \begin{bmatrix} \sigma^2_{r,p}[\tau] & 0 \\ 0 & \sigma^2_{p,p}[\tau] \end{bmatrix}. \tag{17}$$

In a single frame, the node transmits k packets (10 to be exact), some of which can be lost. We shall never know the RSSI values of the lost packets. Therefore, in computing the average RSSI value for that specific frame, we have to take into consideration the RSSI values of the received packets only. The error arising from this approximation we can model as a measurement error. This error can be approximated by the variance of the received packets. The smaller the variance, the more similar are the RSSI values of the received packets, in which case, it is plausible to assume that the RSSI values of the lost packets resemble the RSSI values of the received packets. The larger the variance, the more dissimilar the RSSI values of the received packets, and, as a result, the more dissimilar the lost packets can be from the received packets. Consequently:

$$\sigma^2_{r,m}[\tau] = \frac{1}{k-1} \sum_{i=1}^{k} (r_i - \overline{r}_\tau)^2, \tag{18}$$

where $\overline{r}_\tau$ is the mean RSSI value of frame τ. In a single frame, we have only a single value for p, as PDR is a ratio term. To compute the associated measurement error, we can take into account the fact that $\mathbf{r}$ and $\mathbf{p}$ are correlated in each frame, since the statistics of the latter are directly determined by the statistics of the former. This relationship is encoded by the correlation coefficient, as we already highlighted in Equation (3) and experimentally determined (refer to Figure 6 and Table 1). We can make use of the correlation coefficient to think as if the PDR in the τ's frame has a variance:

$$\sigma_p = \frac{E\left\{(\mathbf{r} - \mu_r)(\mathbf{p} - \mu_p)\right\}}{\rho_{pr}\sigma_p}, \tag{19}$$

where ρ_{rp} is the correlation coefficient. In a single frame, we have the statistics of $\mathbf{r}$. So, it is possible to express Equation (19), in terms of conditional expected values. Distributing the numerator of the right term yields: $E\{\mathbf{rp}\} - \mu_r\mu_p$. Moreover, $E\{\mathbf{rp}\} = \sum_{r\in\mathbf{r}} \sum_{p\in\mathbf{p}} (rp) P(r,p) = \sum_{r\in\mathbf{r}} r \left(\sum_{p\in\mathbf{p}} pP(p|r)\right) P(r)$. The bracket term: $\left(\sum_{p\in\mathbf{p}} pP(p|r)\right)$ is the conditional expected value of $\mathbf{p}$ given $\mathbf{r} = r$. In summary:

$$\sigma^2_{p,m}[\tau] = \frac{\left(\sum_{r\in\mathbf{r}[\tau]} E\{\mathbf{p}|\mathbf{r}[\tau] = r\} rP(r) - \overline{r}_\tau E\{\mathbf{p}|\overline{r}_\tau\}\right)^2}{\sigma^2_{r,m}[\tau]\rho_{rp}}, \tag{20}$$

where $E\{\mathbf{p}|\mathbf{r}[\tau] = r\}$ is the conditional expected value of $\mathbf{p}$ given $\mathbf{r} = r$; $P(r)$ and $E\{\mathbf{p}|\overline{r}_\tau\}$ are the probability of r and the conditional expected value of $\mathbf{p}$, respectively. All the terms on the right side of Equation (20) can be determined from Figure 6. Finally, the measurement covariance error is expressed as:

$$R[\tau] = \begin{bmatrix} \sigma^2_{r,m}[\tau] & cov(r,p) \\ cov(r,p) & \sigma^2_{p,m}(\tau) \end{bmatrix}, \tag{21}$$

Table 3. The Memory Footprint and Computational Complexity of the Different Algorithms

	LL	RSSI	MXMAC	KMF
ROM (bytes)	122	158	5,498	4,876
RAM (bytes)	8	12	118	98
execution time (ms)	—	—	16 ± 0.03	26 ± 0.05

where $cov(\mathbf{r}, \mathbf{p})$ is the covariance between $\mathbf{r}$ and $\mathbf{p}$. With $Q[\tau]$ and $R[\tau]$ in place, it is now possible to compute the Kalman coefficient for τ, and with it, to predict the RSSI and the PDR of the future $(\tau + 1)$ frame.

7 EVALUATION

We implemented our handover-triggering algorithm (KMF) and integrated it with the MXMAC protocol [11]. It runs in a TinyOS runtime environment on the TelosB platform. We also implemented four additional proposed handover-triggering algorithms to make an objective comparison. We summarise these algorithms as follows:

- **Single Packet Failure (SPF)** [35] [24]: Triggers a handover upon a single packet failure.
- **Link Loss (LL)** [54]: Combines consecutive failure and packet failure rate to trigger a handover. Thus, if n packets continuously failed or the packet failure rate falls below a set threshold f within a specified duration, then it triggers a handover.
- RSSI threshold based algorithm (or simply, RSSI): Triggers a handover if the average RSSI value of successively received ACK packets drops below a set threshold [16].
- MXMAC [11]: Employs a normalized LMS filter for predicting link quality fluctuation using the mean RSSI values of received ACK packets.

To evaluate the performance of our algorithm, we conducted a series of experiments using the MobiLab testbed [45]. In our setup, the testbed consisted of 5 static TelosB nodes deployed in a straight line with a 5 m separating distance between them and a mobile node carried by a robot. We deployed the testbed in a lobby, a corridor, and outdoors. The decision to transfer a communication is made by the node carried by the robot. To draw a comparable conclusion for the other handover triggering algorithms, we first launched a large number of preliminary experiments and carried out an in-depth analysis of the received packets. Our aim was to calibrate the parameters for each algorithm.[4] Afterwards, we executed and repeated each experiment ten times. During each experiment, the robot was moving from one end of the deployment area to the other in a straight line, at a constant speed (approximately 0.13 $\mathrm{m\,s^{-1}}$), whilst the transmitter carried by the robot transmitted packets in burst. The IPI is set to 10 ms, which is the minimum interval between two outgoing packets that is currently supported by the TinyOS implementation. The transmission power is set to −25 dBm.

7.1 Memory Footprint and Computational Complexity

Table 3 shows the memory footprint and computational complexity in terms of execution time for all algorithms we implemented. The additional memory overhead is mainly due to the implementation of the handover trigger algorithms and the link quality metrics cached in RAM. SPF

[4]For example, the RSSI threshold and the LMS algorithm require a predefined threshold to achieve 90% packet success rate. This threshold value is environment dependent (−75 dBm in Reference [18], −87 dBm in Reference [26], and −80 dBm in Reference [44]). For more details, refer to our previous work [46].

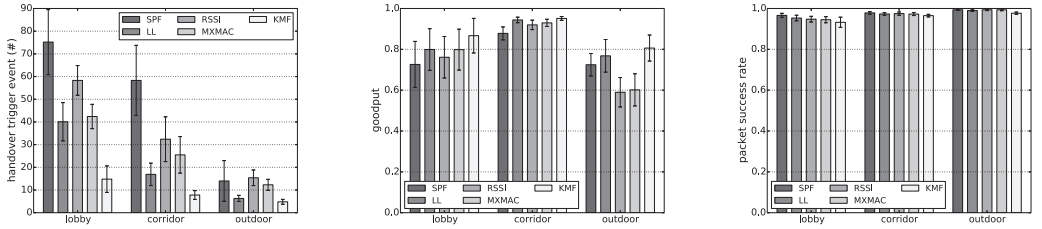

(a) (b) (c)

Fig. 11. Evaluation of the five algorithms in terms of: (a) Number of handover events. (b) Goodput. (c) PSR.

introduces almost no additional memory cost when integrated with MX-MAC. So, it can be taken as a baseline. For the current implementation of KMF, it utilizes 4,876 more bytes in ROM and 98 more bytes in RAM. However, KMF consumes slightly less memory than the original design of MX-MAC. Moreover, compared to the overall available memory in the TelosB platform (48 KB flash and 10 KB RAM), the additional memory overhead is not appreciable.

The computational overhead is mainly due to the execution of the link quality estimation and the prediction algorithm. Therefore, we programmed the TelosB platform to execute each handover trigger algorithm 10,000 times in a single test and then we repeated 100 tests. Additionally, the execution time of link quality estimation depends on the window size, so we fixed this parameter to 10. Then we calculated the average value as the execution time. The link quality estimator in KMF is executed for each packet transmission and the Kalman Filter prediction is made after the transmission of 10. Totally these two computations take ca. 26 ms. Considering the minimum IPI 10 ms, the computation can be completed without introducing a significant latency. As far as energy consumption is concerned, the computation consumes much less energy compared to the cost of transmitting 10 packets. For example, the CC2420 radio consumes 17.4 mA at 0 dBm when in transmission mode [21], while the MCU (MSP430) consumes 1.8 mA in busy mode [8]. To transmit one packet (which is typically 45 bytes in the TinyOS environment), it consumes 0.08 mJ. To transmit 10 packets, this would amount to 0.8 mJ. And to do one round of Kalman filter computation (which is carried out after the transmission of 10 packets), it takes 0.14 mJ.

7.2 Handover Trigger Event

A *handover trigger event* is generated when a handover triggering algorithm initiates a handover as a result of a "belief" by the former that a deterioration in the link quality leads to a disconnection or that the packet loss rate is below a specified threshold. It is a measure of the sensitivity of the triggering algorithm. A highly sensitive algorithm leads to a frequent attempt to transfer a communication to an alternative relay node, and may cause a high handover cost. As most commercially available transceivers are low-powered and low-cost, the RSSI values of received ACK packets may fluctuate for a brief period of time despite the low speed of the robot. In other words, a fluctuation in the RSSI values of received ACK packets may not necessarily indicate the potential disconnection of an established link. Thus, the handover triggering algorithm should be tolerant to such transient variations of link quality, otherwise it may lead to a ping-pong handover problem, unnecessarily increasing packet transmission latency and power consumption. Moreover, a mobile transmitter may not be successful in finding a new relay node whenever a handover is initiated, in which case it may waste resources in searching for relay nodes. Figure 11(a) suggests that our algorithms (KMF) generated a significantly less number of trigger events than all the other algorithms, because it was able to filter transient link fluctuations more efficiently than the other solutions,

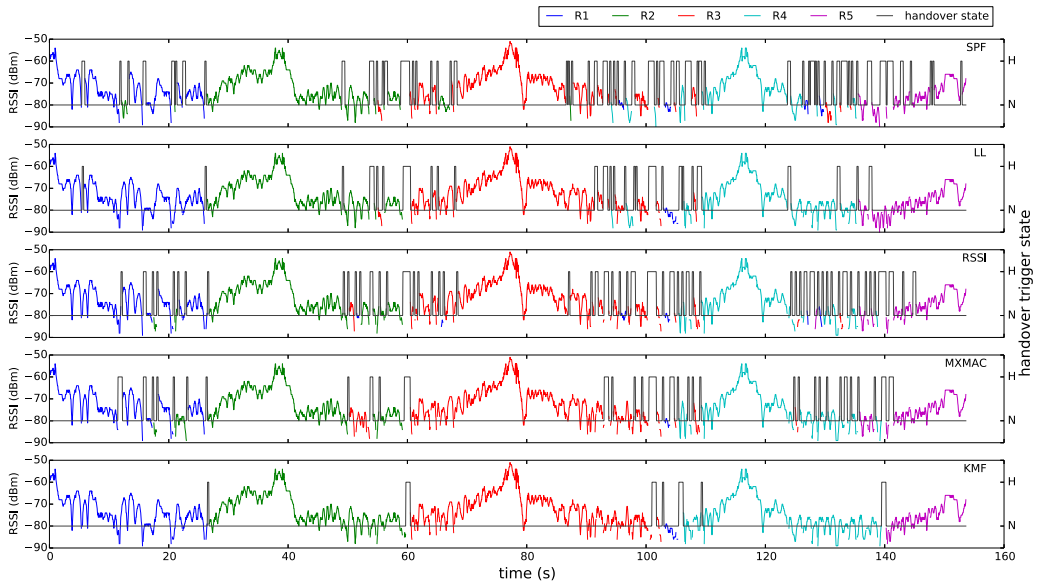

Fig. 12. Comparison of the resulting handover oscillations of different link quality estimation approaches. The maxima of the coloured signals indicate that the robot was approximately at the same position as the relay nodes. **H** indicates that a request for a handover was made by the mobile node and **N** indicates that no request was made.

particularly, in the indoor environments (lobby and corridor). The SPF algorithm performed worst due to its reliance on a single packet failure to trigger a handover.

7.3 Goodput and Packet Success Rate

We define the *goodput* as the ratio of the number of successfully transmitted data packets to the maximum data packets that can be transmitted in an ideal link during the same transmission period:

$$Goodput = \frac{N_{success}}{N_{ideal}}.$$

As shown in Figure 11(b), KMF gains the highest goodput overall in different environments. The reason is its high data packet transmission efficiency. Furthermore, KMF is the only algorithm the average goodput of which is above 80%. It can be seen in Figure 11(c) that, compared to the other algorithms, the performance of KMF degraded a little bit in terms of packet success rate. It achieved 93.2%, 96.5%, and 97.7% for lobby, corridor, and outdoor, respectively. The reason for the relatively low performance in this respect is its higher tolerance of transient packet failures.

7.4 Simulation

To compare the performance of all the handover algorithms under an identical condition, we let the robot move from one end of the deployment environment to another while communicating with the relay nodes (without any handover). During this time, all the link quality metrics were recorded. After the experiment, we fed the link quality metrics to the algorithms to observe how they would react to the link quality fluctuations and recorded the time points at which they triggered a handover.

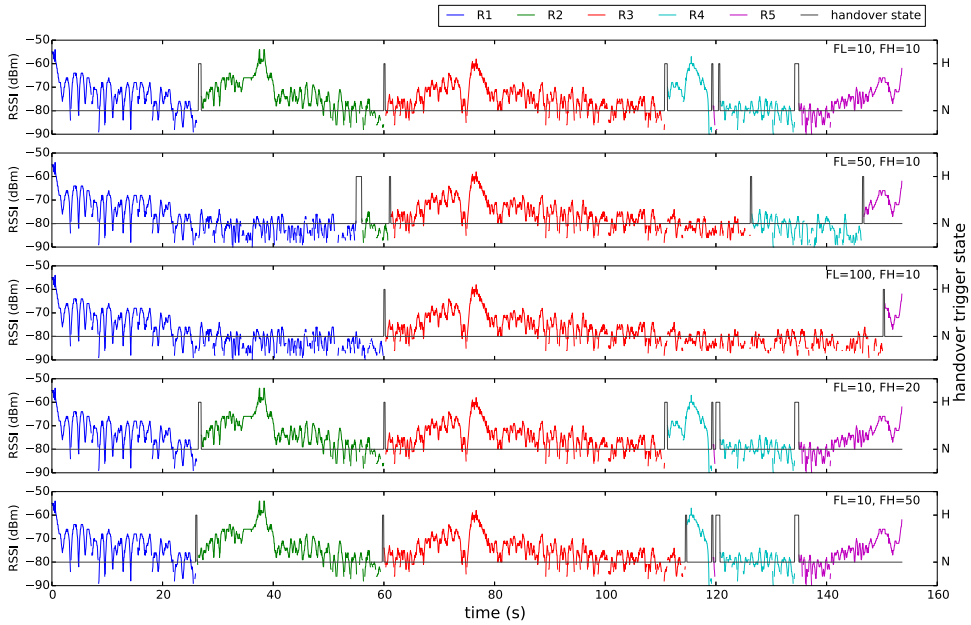

Fig. 13. Handover oscillations for different Kalman Filter parameters. **H** indicates the firing of a handover request by the mobile node, and **N** the absence of such a request.

Figure 12 compares the handover oscillations arising from implementing the different link quality estimation techniques. The coloured lines illustrate how the transmitter carried by the robot maintained a steady communication link by employing the handover-triggering algorithms. The vertical bars display the frequency of the attempts to transfer a communication as a result of a perceived change in the link quality.

Triggering a handover request at the appropriate time is essential to avoid unnecessary oscillations. If the handover trigger algorithm is too sensitive to link quality variations, then a high number of handover events are experienced and, consequently, the handover cost (signalling overhead, latency, etc.) is correspondingly high. On the contrary, if the algorithm is too tolerant to the link dynamics and fails to trigger a handover on time, then the node may suffer from a considerable packet loss. As can be seen in the figure, our approach (KMF) reduced the number of handover triggers considerably (by about 23% compared to SPF and by 12% compared to MXMAC).

7.5 Analysis of Model Parameter Selection

The Kalman Filter we apply for estimating handover triggering events relies on two essential parameters, namely, the frame length for establishing the system state and the past history for predicting the system state. Apparently, a large amount of data is useful for establishing reliable statistics in both cases, but the time and resources needed to collect, process, and store the data are correspondingly high. The aim of this subsection is to closely examine this tradeoff.

7.5.1 Frame Length. The **frame length (FL)** is the number of packets used to calculate the system state, $[r[\tau], p[\tau]]^T$. A long FL signifies, on the one hand, to a reliable statistics for a fine-grained estimation, and, on the other, to a correspondingly long time to reach at a decision to trigger a handover event. The effect of this may be manifested in terms of a significant packet loss if the link quality fluctuates considerably. If we fix the **Frame History (FH)** ($FH = 10$) and

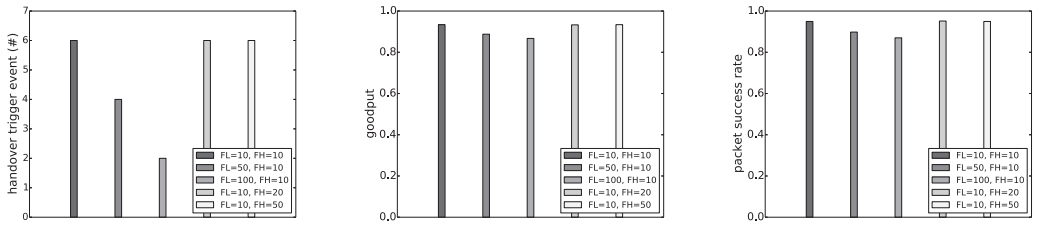

Fig. 14. The performance of different values of the Kalman Filter parameters: (a) The number of handover events. (b) Goodput. (c) PSR.

choose different FL (namely, $FL = \{10, 50, 100\}$), then we can observe that (refer to Figure 13) the time elapses for the first trigger event to occur increases correspondingly: 25 s, 55 s, and 60 s. In other words, the number of handover trigger events decreases as FL increases. As might be expected, the goodput and packet success rate drop also when FL becomes large.

7.5.2 Frame History. The FH is the number of past frames used to predict the future system state (the parameter a in Equation (12)). One may assume that the larger the value of FH, the slower will be the update rate of a. However, the simulation result in Figure 14 suggests that the impact of FH is inappreciable. We suspect that the optimal frame history depends on the speed of the mobile node and the inter-packet interval of the transmission. This will be one of the open issues we shall investigate in future.

8 CONCLUSION

Understanding the characteristics of link quality fluctuation is critical for deploying wireless sensor networks for practical applications. Previous studies have already shown how decisions pertaining to deployment density and placement of sensor nodes, topology, transmission power control, and protocol design can be influenced by and benefit from knowledge of link quality fluctuations. Most existing studies, however, focus on static deployments where the sensor nodes remain stationary once deployed or move only slowly over time.

In our study, we complemented existing work by characterising link quality fluctuation in mobile scenarios, focusing on slow movements and employing different link quality metrics to provide different perspectives. The results of our experiments clearly indicate that wireless links are highly sensitive to mobility and predicting the existence and duration of *connected* and *transitional* regions is more difficult. Having said this, our study also shows that by combining the different link quality metrics, a more reliable estimation can be possible. As a demonstration of this, we combined the RSSI values of incoming (ACK) packets with PDR using a Kalman Filter to estimate link quality fluctuation and to trigger a seamless handover. Compared to the state of the art, our approach could improve link quality prediction by up to 12%.

REFERENCES

[1] Cedric Adjih, Emmanuel Baccelli, Eric Fleury, Gaetan Harter, Nathalie Mitton, Thomas Noel, Roger Pissard-Gibollet, Frederic Saint-Marcel, Guillaume Schreiner, Julien Vandaele, et al. 2015. FIT IoT-LAB: A large scale open experimental IoT testbed. In *Proceedings of the IEEE 2nd World Forum on Internet of Things (WF-IoT'15)*. IEEE, 459–464.

[2] Nadeem Ahmed, Salil S. Kanhere, and Sanjay Jha. 2016. On the importance of link characterization for aerial wireless sensor networks. *IEEE Commun. Mag.* 54, 5 (2016), 52–57.

[3] Nouha Baccour, Anis Koubaa, Luca Mottola, Marco Antonio Zuniga, Habib Youssef, Carlo Alberto Boano, and Mário Alves. 2012. Radio link quality estimation in wireless sensor networks: A survey. *ACM Trans. Sens. Netw.* 8, 4 (2012), 34.

[4] Nouha Baccour, Anis Koubâa, Habib Youssef, Maissa Ben Jamâa, Denis Do Rosario, Mário Alves, and Leandro B. Becker. 2010. F-lqe: A fuzzy link quality estimator for wireless sensor networks. In *Proceedings of the International Conference on Embedded Wireless Systems and Networks (EWSN'10)*. Springer, 240–255.
[5] Sravani Challa, Ashok Kumar Das, Vanga Odelu, Neeraj Kumar, Saru Kumari, Muhammad Khurram Khan, and Athanasios V. Vasilakos. 2018. An efficient ECC-based provably secure three-factor user authentication and key agreement protocol for wireless healthcare sensor networks. *Comput. Electr. Eng.* 69 (2018), 534–554.
[6] Diana Cogan, Javad Birjandtalab, Mehrdad Nourani, Jay Harvey, and Venkatesh Nagaraddi. 2017. Multi-biosignal analysis for epileptic seizure monitoring. *Int. J. Neur. Syst.* 27, 01 (2017), 1650031.
[7] LAN/MAN Standards Committee et al. 2006. IEEE standard for information technology telecommunications and information exchange between systems local and metropolitan area networks specific requirements. Part 15.4: Wireless Medium Access Control (MAC) and Physical Layer (PHY) specifications for Low-Rate Wireless Personal Area Networks (LR-WPANs). *IEEE Std* 802 (2006).
[8] Moteiv Corporation. 2004. Telos:Ultra Low Power IEEE 802.15.4 Compliant Wireless Sensor Module. Retrieved from http://www2.ece.ohio-state.edu/ bibyk/ee582/telosMote.pdf.
[9] Waltenegus Dargie. 2017. *Principles and Applications of Ubiquitous Sensing*. John Wiley & Sons.
[10] Waltenegus Dargie and Christian Poellabauer. 2010. *Fundamentals of Wireless Sensor Networks: Theory and Practice*. John Wiley & Sons.
[11] Waltenegus Dargie and Jianjun Wen. 2014. A seamless handover for WSN Using LMS filter. In *Proceedings of the IEEE Conference on Local Computer Networks (LCN'14)*. IEEE, 442–445.
[12] Behnam Dezfouli, Marjan Radi, Shukor Abd Razak, Tan Hwee-Pink, and Kamalrulnizam Abu Bakar. 2015. Modeling low-power wireless communications. *J. Netw. Comput. Appl.* 51 (2015), 102–126. DOI: https://doi.org/10.1016/j.jnca.2014.02.009
[13] Qian Dong and Waltenegus Dargie. 2012. Evaluation of the reliability of RSSI for indoor localization. In *Proceedings of the 2012 International Conference on Wireless Communications in Underground and Confined Areas*. IEEE, 1–6.
[14] Muhammad Faheem and Vehbi Cagri Gungor. 2018. MQRP: Mobile sinks-based QoS-aware data gathering protocol for wireless sensor networks-based smart grid applications in the context of industry 4.0-based on internet of things. *Fut. Gener. Comput. Syst.* 82 (2018), 358–374.
[15] Hossein Fotouhi, Mário Alves, Anis Koubaa, and Nouha Baccour. 2010. On a reliable handoff procedure for supporting mobility in wireless sensor networks. In *Proceedings of the International Workshop on Real-Time Networks (RTN'10)*.
[16] Hossein Fotouhi, Marco Zúñiga, Mário Alves, Anis Koubâa, and Pedro Marrón. 2012. Smart-hop: A reliable handoff mechanism for mobile wireless sensor networks. In *Wireless Sensor Networks*. Springer, 131–146.
[17] Ruan D. Gomes, Diego V. Queiroz, Abel C. Lima Filho, Iguatemi E. Fonseca, and Marcelo S. Alencar. 2017. Real-time link quality estimation for industrial wireless sensor networks using dedicated nodes. *Ad Hoc Netw.* 59 (2017), 116–133.
[18] Antonio Gonga, Olaf Landsiedel, and Mikael Johansson. 2011. MobiSense: Power-efficient micro-mobility in wireless sensor networks. In *Proceedings of the International Conference on Distributed Computing in Sensor Systems (DCOSS'11)*. IEEE, 1–8.
[19] Hooman Hafezi, Timothy L. Robertson, Greg D. Moon, Kit-Yee Au-Yeung, Mark J. Zdeblick, and George M. Savage. 2015. An ingestible sensor for measuring medication adherence. *IEEE Trans. Biomed. Eng.* 62, 1 (2015), 99–109.
[20] Mohammad Mehedi Hassan, Kai Lin, Xuejun Yue, and Jiafu Wan. 2017. A multimedia healthcare data sharing approach through cloud-based body area network. *Fut. Gener. Comput. Syst.* 66 (2017), 48–58.
[21] Texas Instruments. 2013. 2.4 GHz IEEE 802.15.4/ZigBee-ready RF Transceiver. *Reference SWRS041c* (2013).
[22] Kourosh Kalantar-Zadeh, Nam Ha, Jian Zhen Ou, and Kyle J. Berean. 2017. Ingestible sensors. *ACS Sens.* 2, 4 (2017), 468–483.
[23] J. Ko and M. Chang. 2015. MoMoRo: Providing mobility support for low-power wireless applications. *IEEE Syst. J.* 9, 2 (Jun. 2015), 585–594. DOI: https://doi.org/10.1109/JSYST.2014.2299592
[24] Romain Kuntz, Julien Montavont, and Thomas Noël. 2013. Improving the medium access in highly mobile wireless sensor networks. *Telecommun. Syst.* 52, 4 (2013), 2437–2458.
[25] Michael A. Leabman and Gregory Scott Brewer. 2018. Receivers for wireless power transmission. US Patent 9,912,199.
[26] K. S. A. P. Levis. 2006. RSSI is under appreciated. In *Proceedings of the 3rd Workshop on Embedded Networked Sensors*, Vol. 3031. 239242.
[27] Philip Levis, Sam Madden, Joseph Polastre, Robert Szewczyk, Kamin Whitehouse, Alec Woo, David Gay, Jason Hill, Matt Welsh, Eric Brewer, et al. 2005. Tinyos: An operating system for sensor networks. In *Ambient Intelligence*. Springer, 115–148.
[28] Chieh-Jan Mike Liang, Nissanka Bodhi Priyantha, Jie Liu, and Andreas Terzis. 2010. Surviving wi-fi interference in low power zigbee networks. In *Proceedings of the 8th ACM Conference on Embedded Networked Sensor Systems*. ACM, 309–322.

[29] Shan Lin, Fei Miao, Jingbin Zhang, Gang Zhou, Lin Gu, Tian He, John A. Stankovic, Sang Son, and George J. Pappas. 2016. ATPC: Adaptive transmission power control for wireless sensor networks. *ACM Trans. Sens. Netw.* 12, 1 (2016), 6.

[30] Emiliano Miluzzo, Xiao Zheng, Kristóf Fodor, and Andrew T. Campbell. 2008. Radio characterization of 802.15. 4 and its impact on the design of mobile sensor networks. In *Proceedings of the European Conference on Wireless Sensor Networks*. Springer, 171–188.

[31] Mobashir Mohammad, XiangFa Guo, and Mun Choon Chan. 2016. Oppcast: Exploiting spatial and channel diversity for robust data collection in urban environments. In *Proceedings of the 15th International Conference on Information Processing in Sensor Networks*. IEEE Press, 19.

[32] Lama Nachman, Jonathan Huang, Junaith Shahabdeen, Robert Adler, and Ralph Kling. 2008. Imote2: Serious computation at the edge. In *Proceedings of the International Wireless Communications and Mobile Computing Conference (IWCMC'08)*. IEEE, 1118–1123.

[33] John Neter, Michael H. Kutner, Christopher J. Nachtsheim, and William Wasserman. 1996. *Applied Linear Statistical Models*. Vol. 4. Irwin, Chicago.

[34] Homayoun Nikookar and Homayoun Hashemi. 1993. Statistical modeling of signal amplitude fading of indoor radio propagation channels. In *Proceedings of the 2nd International Conference on Universal Personal Communications,* Vol. 1. IEEE, 84–88.

[35] Georgios Z. Papadopoulos, Vasileios Kotsiou, Antoine Gallais, Periklis Chatzimisios, and Thomas Noël. 2015. Wireless medium access control under mobility and bursty traffic assumptions in WSNs. *Mobile Netw. Appl.* 20, 5 (2015), 649–660.

[36] Sandeep Pirbhulal, Heye Zhang, Wanqing Wu, Subhas Chandra Mukhopadhyay, and Yuan-Ting Zhang. 2018. Heartbeats based biometric random binary sequences generation to secure wireless body sensor networks. *IEEE Trans. Biomed. Eng.* 65, 12 (2018), 2751–2759.

[37] Joseph Polastre, Robert Szewczyk, and David Culler. 2005. Telos: Enabling ultra-low power wireless research. In *Proceedings of the 4th International Symposium on Information Processing in Sensor Networks (IPSN'05)*. IEEE, 364–369.

[38] Ju Ren, Yaoxue Zhang, Kuan Zhang, and Xuemin Shen. 2016. Adaptive and channel-aware detection of selective forwarding attacks in wireless sensor networks. *IEEE Trans. Wireless Commun.* 15, 5 (2016), 3718–3731.

[39] Amit Samanta, Samaresh Bera, and Sudip Misra. 2018. Link-quality-aware resource allocation with load balance in wireless body area networks. *IEEE Syst. J.* 12, 1 (2018), 74–81.

[40] Nadia Shakoor, Scott Lee, and Todd C. Mockler. 2017. High throughput phenotyping to accelerate crop breeding and monitoring of diseases in the field. *Curr. Opin. Plant Biol.* 38 (2017), 184–192.

[41] Zhengguo Sheng, Chinmaya Mahapatra, Chunsheng Zhu, and Victor Leung. 2015. Recent advances in industrial wireless sensor networks towards efficient management in IoT. *IEEE Access* 3 (2015), 622–637.

[42] Bruno Silva, Roy M. Fisher, Anuj Kumar, and Gerhard P. Hancke. 2015. Experimental link quality characterization of wireless sensor networks for underground monitoring. *IEEE Trans. Industr. Inf.* 11, 5 (2015), 1099–1110.

[43] Kannan Srinivasan, Prabal Dutta, Arsalan Tavakoli, and Philip Levis. 2010. An empirical study of low-power wireless. *ACM Trans. Sens. Netw.* 6, 2 (2010), 16.

[44] Kannan Srinivasan, Maria A. Kazandjieva, Saatvik Agarwal, and Philip Levis. 2008. The β-factor: Measuring wireless link burstiness. In *Proceedings of the ACM Conference on Embedded Networked Sensor Systems (SenSys'08)*. ACM, 29–42.

[45] Jianjun Wen, Zeeshan Ansar, and Waltenegus Dargie. 2016. MobiLab: A testbed for evaluating mobility management protocols in WSN. In *Testbeds and Research Infrastructures for the Development of Networks and Communities*. Springer, 49–58.

[46] J. Wen and W. Dargie. 2018. A handover triggering algorithm for managing mobility in WSNs. In *Proceedings of the 2018 21st International Conference on Information Fusion (FUSION'18)*. 1646–1652. DOI: https://doi.org/10.23919/ICIF.2018.8455472

[47] Jianjun Wen and Waltenegus Dargie. 2018. A mobility management protocol for wireless sensor networks. In *Proceedings of the 2018 IEEE Symposium on Computers and Communications (ISCC'18)*. IEEE, 00390–00396.

[48] Wei Xiong, Xiaoya Hu, and Tao Jiang. 2016. Measurement and characterization of link quality for IEEE 802.15. 4-compliant wireless sensor networks in vehicular communications. *IEEE Trans. Industr. Inf.* 12, 5 (2016), 1702–1713.

[49] Shusen Yang, Usman Adeel, Yad Tahir, and Julie A McCann. 2017. Practical opportunistic data collection in wireless sensor networks with mobile sinks. *IEEE Trans. Mobile Comput.* 16, 5 (2017), 1420–1433.

[50] Dingwen Yuan, Salil S. Kanhere, and Matthias Hollick. 2017. Instrumenting wireless sensor networks—A survey on the metrics that matter. *Perv. Mobile Comput.* 37 (2017), 45–62.

[51] Tang Zhiyong and Waltenegus Dargie. 2010. A mobility-aware medium access control protocol for wireless sensor networks. In *Proceedings of the IEEE Global Communications Conference Workshops (Globecom Workshops'10)*. IEEE, 109–114.

[52] Gang Zhou, Tian He, Sudha Krishnamurthy, and John A Stankovic. 2004. Impact of radio irregularity on wireless sensor networks. In *Proceedings of the 2nd International Conference on Mobile Systems, Applications, and Services*. ACM, 125–138.

[53] Zinon Zinonos, Chrysostomos Chrysostomou, and Vasos Vassiliou. 2014. Wireless sensor networks mobility management using fuzzy logic. *Ad Hoc Netw.* 16 (2014), 70–87.

[54] Zinon Zinonos, Vasos Vassiliou, and Chrysostomos Chrysostomou. 2013. Handoff triggering for wireless sensor networks with performance needs. In *Proceedings of the IEEE Symposium on Computers and Communications (ISCC'13)*. IEEE, 000982–000988.

Received December 2019; revised November 2020; accepted January 2021